

Evaluation of Fe- β Ga₂O₃ for Photoconductive Semiconductor Switching

Dowling, Karen M.; Chatterjee, Bikramjit; Ghandiparsi, Soroush; Shao, Qinghui; Varley, Joel; Schneider, Joseph D.; Chapin, Caitlin; Gottlieb, Miranda S.; Leos, Laura; Sword, Michael

DOI

[10.1109/TED.2024.3352528](https://doi.org/10.1109/TED.2024.3352528)

Publication date

2024

Document Version

Final published version

Published in

IEEE Transactions on Electron Devices

Citation (APA)

Dowling, K. M., Chatterjee, B., Ghandiparsi, S., Shao, Q., Varley, J., Schneider, J. D., Chapin, C., Gottlieb, M. S., Leos, L., Sword, M., Harrison, S., & Voss, L. (2024). Evaluation of Fe- β Ga₂O₃ for Photoconductive Semiconductor Switching. *IEEE Transactions on Electron Devices*, 71(3), 1535-1540. <https://doi.org/10.1109/TED.2024.3352528>

Important note

To cite this publication, please use the final published version (if applicable). Please check the document version above.

Copyright

Other than for strictly personal use, it is not permitted to download, forward or distribute the text or part of it, without the consent of the author(s) and/or copyright holder(s), unless the work is under an open content license such as Creative Commons.

Takedown policy

Please contact us and provide details if you believe this document breaches copyrights. We will remove access to the work immediately and investigate your claim.

Green Open Access added to TU Delft Institutional Repository

'You share, we take care!' - Taverne project

<https://www.openaccess.nl/en/you-share-we-take-care>

Otherwise as indicated in the copyright section: the publisher is the copyright holder of this work and the author uses the Dutch legislation to make this work public.

Evaluation of Fe- β Ga₂O₃ for Photoconductive Semiconductor Switching

Karen M. Dowling¹, Member, IEEE, Bikramjit Chatterjee², Soroush Ghandiparsi, Qinghui Shao¹, Joel Varley, Joseph D. Schneider², Caitlin Chapin², Miranda S. Gottlieb, Laura Leos², Michael Sword, Sara Harrison², Member, IEEE, and Lars Voss²

Abstract—We present iron-doped beta gallium oxide (Fe- β Ga₂O₃) as a candidate for photoconductive semiconductor switches (PCSSs) with sub-bandgap light. From a commercially available Fe- β Ga₂O₃ wafer, we first did material characterization. This included measurements of absorption coefficient and dopant composition, carrier activation energy up to 200 °C, break down field of planar electrodes (limited from material passivation), and free carrier recombination lifetime, and thermal effects up to 203 °C on photocurrent with a 447 nm light emitting diode (LED) source. We then demonstrated pulsed operation of a Fe- β Ga₂O₃ PCSS under different sub-bandgap wavelengths (355, 532, and 1064 nm) and sub-ns pulses. Fe- β Ga₂O₃ is a candidate for high temperature PCSS with 355 nm responsivity of 7×10^{-7} A-cm/W-kV at room temperature and up to 5.5×10^{-4} A-cm/W-kV at 200 °C. From these investigations, we discuss a simple trap model to describe the illumination process of the PCSS. Fe- β Ga₂O₃ has a high breakdown field and has moderate responsivity characteristics, but the dark current at high temperature leads to low photo-to-dark current ratio (PDCR). Regardless, we verify its potential as a PCSS material for harsh environment applications.

Index Terms—Fe-doping, gallium oxide, photoconductive switch, sub bandgap illumination.

I. INTRODUCTION

PHOTOCONDUCTIVE semiconductor switches (PCSSs) have been used regularly for high voltage, low leakage power handling which is difficult to achieve in electrically

Manuscript received 31 August 2023; revised 27 October 2023 and 1 December 2023; accepted 6 December 2023. Date of publication 22 January 2024; date of current version 1 March 2024. This work was supported in part by the U.S. Department of Energy through the Lawrence Livermore National Laboratory Contract under Grant LLNL-JRNL-853779, in part by the Laboratory Directed Research and Development Program under Project 22-SI-003, and in part by the Joint Fuze Technology Program under Grant 20-G-029. The review of this article was arranged by Editor D. N. Nath. (Corresponding author: Lars Voss.)

Karen M. Dowling was with the Materials Engineering Division, Lawrence Livermore National Laboratory, Livermore, CA 94550 USA. She is now with the Microelectronics Department, Faculty of Electrical Engineering, Math and Computer Science, Delft Institute of Technology, 2611LS Delft, The Netherlands (e-mail: k.m.dowling@tudelft.nl).

Bikramjit Chatterjee, Soroush Ghandiparsi, Qinghui Shao, Joel Varley, Joseph D. Schneider, Caitlin Chapin, Miranda S. Gottlieb, Laura Leos, Michael Sword, Sara Harrison, and Lars Voss are with the Materials Engineering Division, Lawrence Livermore National Laboratory, Livermore, CA 94550 USA (e-mail: voss5@llnl.gov).

Color versions of one or more figures in this article are available at <https://doi.org/10.1109/TED.2024.3352528>.

Digital Object Identifier 10.1109/TED.2024.3352528

gated devices. They are typically designed to operate for various applications from 1 to 100 kV blocking voltage in a compact geometry with fast rise and fall times and thus higher switching frequencies. This has led to PCSS adoption in various areas, including directed energy pulse generators [1], ultrawideband radar [1], and distributed energy resource systems [2]. In particular, wide bandgap and ultrawide bandgap materials are excellent candidates for high energy density PCSS due to their ability to block large voltages with high electric field strength > 2 MV/cm [1]. To overcome the need for high energy photon sources as an optical gate, deep dopants can be used to enable sub-bandgap triggering of these devices, such as that of vanadium in silicon carbide [3] and nitrogen in diamond [4]. While diamond has shown excellent sub-bandgap performance with field-scaled photoresponsivity (R/E) around 10^{-5} A-cm/W-kV [4], [5], this material is still quite expensive and substrates are relatively small and difficult to process. While the critical electric field strength of diamond is ~ 10 MV/cm, gallium oxide (Ga₂O₃) is also an emerging material for power semiconductors with similar field strength of ~ 6 MV/cm, and 2-in substrates are readily available for processing [6], [7], [8]. In addition, Fe has been identified as a deep acceptor in Ga₂O₃, around 0.7–0.8 eV below the conduction band (CB) minimum which can emit electrons to the CB by sub-bandgap illumination [9], [10], [11], [12], [13], [14], [15]. It has also been found that iridium (Ir) dopants, which originate from the crystal growth process, sit mid-band around 2.2–2.3 eV and are also a source of carrier emission at lower wavelength absorption [16].

Here, we investigate semi-insulating Fe- β Ga₂O₃ for PCSS operation at high temperatures. Our results include a series of optical [spectrophotometry and photoluminescence (PL)], electro-thermal, and photocurrent measurements to characterize Fe- β Ga₂O₃ as a PCSS material. Then, we conclude with pulsed measurements of a PCSS vertical device. From this, we extract several material properties and evaluate the photoresponsivity of Fe- β Ga₂O₃ and sub-bandgap illumination conduction with various optical wavelengths. In the discussion we propose a simple trap model that considers the influence of Fe, Ir, and other potential impurities to explain these results.

II. METHODOLOGY

A. Material Characterization

The Fe-Ga₂O₃ samples were semi-insulating (010) β -Ga₂O₃ 1-in wafers around 450 μ m thick [Fig. 1(a)]. Secondary ion

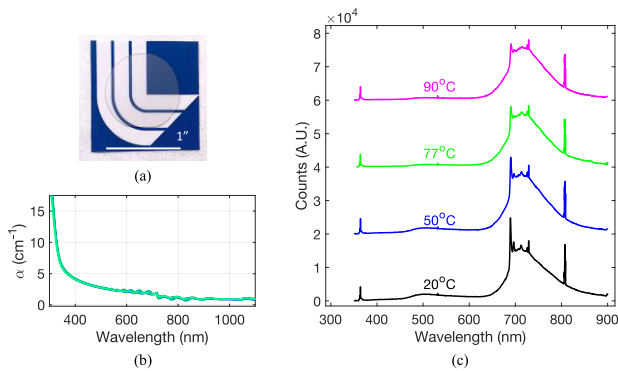


Fig. 1. (a) Optical image of the 1" Fe- β Ga₂O₃ wafer, (b) spectrophotometer measurement of the absorption coefficient from UV to IR, and (c) PL spectrum of the sample with a 355 nm optical source over from room temperature to 90 °C.

TABLE I
ACTIVE IMPURITIES IN THE Fe- β Ga₂O₃ SAMPLES
MEASURED WITH SIMS

Element	SIMS Concentration (atoms/cm ³)	Trap Type	Energy Level (eV)
Fe	1.6x10 ¹⁸	Deep Acceptor	0.7-0.8 eV [11-15]
Si	1.7x10 ¹⁷	Shallow Donor	16 to 36 meV [18]
Ir	1.9x10 ¹⁷	Deep Donor	2.2-2.3 eV [16]

mass spectroscopy (SIMS) results for the three species of interest (Si, Fe, and Ir) are listed in Table I. Si is a shallow dopant which unintentionally dopes Ga₂O₃ to be n-type. Fe is added an order of magnitude higher ($1.6 \times 10^{18} \text{ cm}^{-3}$) to compensate Si ($1.7 \times 10^{17} \text{ cm}^{-3}$) and make the material semi-insulating [17]. Ir was also measured since it is commonly incorporated in the growth process [18]. We performed absorption measurements with a Cary UV-VIS-NIR spectrophotometer (7000 Series) and calculated the absorption coefficient using the method described by Look & Leach [19], across the spectrum from 300 to 1100 nm shown in Fig. 1(b). An increase in the absorption coefficient value is seen in the small wavelengths, close to the bandgap edge. The five spots measured on the wafer (center and four surrounding areas) are in close agreement showing decent uniformity across the wafer.

A Horiba spectrometer was used to capture the PL spectrum of the sample with a 355 nm optical source, measured from 20 °C to 90 °C, shown in Fig. 1(c). The peaks located in the red region (690–800 nm) confirm the presence of Fe traps seen previously in literature [20]. The elevated temperature spectrum at 90 °C shows a small reduction in defect peaks as compared to the room temperature spectrum, and some are no longer observable between 690 and 720 nm. We do not believe this is due to trap repair but is instead a limitation of the PL method at elevated temperatures. Deep energy traps broaden at high temperatures and cause overlapping peaks to smear [21]. While the small temperature increase shows a small effect of the relative peak heights in the data, these results are inconclusive as to the presence of additional deep level traps, and will not be considered further in this study.

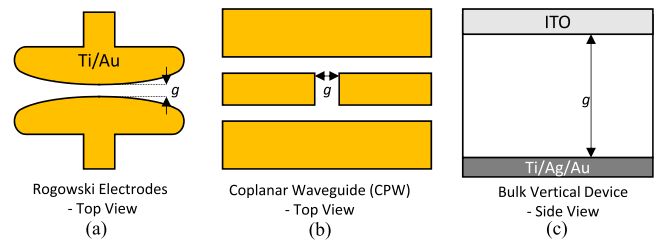


Fig. 2. Electrical test structures fabrication, including (a) Rogowski electrodes for high field measurements designed for electrode gap g . (b) CPW structure with signal trace gap g used for lifetime measurements. (c) Vertical structure used for PCSS responsivity characterization.

B. Test Structures Fabrication

Two planar types of devices were fabricated. First, planar electrodes using a Rogowski profile [22] were designed to support high voltages for electrical characterization of breakdown fields, as shown in Fig. 2(a). This electrode profile avoids premature breakdown due to electric field crowding due to sharp corners but is still subject to semiconductor-dielectric interface limitations. Electrode gaps (g) were designed for 2, 5, 10, and 20 μm spacing. Coplanar waveguides (CPWs), shown in Fig. 2(b), were included for use in high-frequency carrier lifetime measurements with $g = 2, 5, 10,$ and 20 μm . These electrodes were fabricated using a simple liftoff process with negative photoresist (NLOF 2020) and an electron-beam evaporated Ti (10 nm)/Au (150 nm) metal stack annealed at 470 °C for 1 min. Due to the heavily insulated nature of the substrate, contact resistance was not measured. A 1.1 μm polyimide layer was spun, cured, and patterned for passivation. The Rogowski planar electrodes included samples with and without passivation present, and the CPWs were not passivated to ensure impedance matching using according to ground-signal-ground CPW design tools.

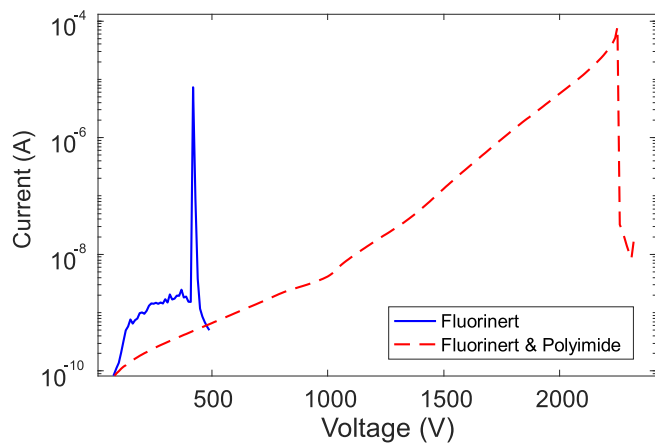
Finally, PCSS measurements were performed with a separate vertical device [Fig. 2(c)]. The device had $4 \times 4 \text{ mm}$ area, $g = 480 \mu\text{m}$, and used an indium tin oxide (ITO) layer as a top transparent electrode and a reflective Ti/Ag/Au electrode on the back.

III. RESULTS

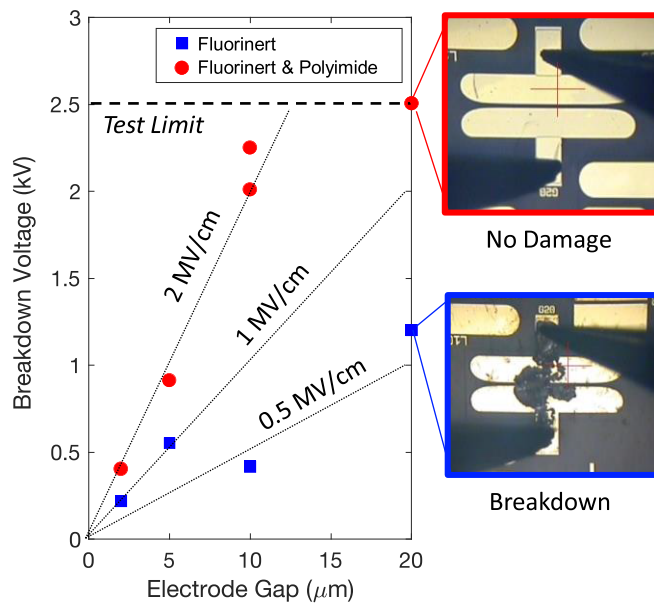
A. Breakdown Field

Rogowski electrodes with and without polyimide passivation were measured to breakdown to get a preliminary understanding of the field handling capability. The sample was placed on a high-voltage probe station in a container of fluorinert to avoid air breakdown. Dark current was monitored using a picoammeter and dc voltage was provided with a Stanford research system (SRS PS370) 2.5 kV supply. Voltage was ramped up in 10 V increments until a high current failure was detected to determine breakdown voltages. One such experiment curve is depicted in Fig. 3(a).

The Rogowski planar device breakdown voltage with respect to device gap variation is plotted in Fig. 3(b), along with dashed guided lines for 0.5–2 MV/cm average electric fields. The devices with passivated polyimide follow the 2 MV/cm trace (with the exception of the largest device



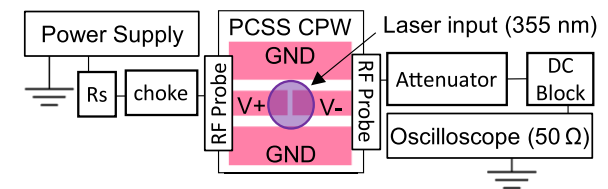
(a)



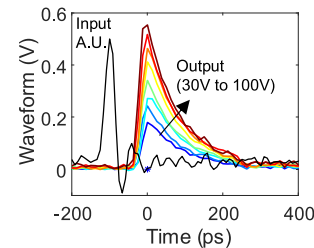
(b)

Fig. 3. Breakdown field measurements on Rogowski electrodes of Fe- β Ga₂O₃. (a) Example current–voltage curve of two $g = 10 \mu\text{m}$ devices, one with polyimide passivation and one without. (b) Breakdown voltages found compared to electrode gap spacing (g), with optical images showing a device which did not breakdown and one that did breakdown.

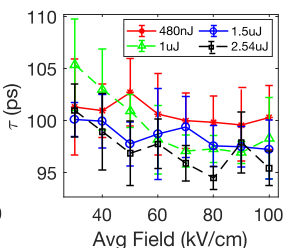
which did not break down due to the equipment supply limit of 2.5 kV). The un-passivated devices, tested only in fluorinert, broke down between 0.5 and 1 MV/cm. These results align with the experimental situation: the planar devices breakdown based on the passivation electric field strength. Polyimide's breakdown field is around 2 MV/cm [23], and fluorinert's breakdown field is only rated by the manufacturer to 180 kV/cm [24]. β Ga₂O₃ devices has been shown in literature to breakdown at 5.3 MV/cm and in theory can go up to 5.8 MV/cm [8], [25], [26], but these structures have stronger dielectric materials (~ 10 MV/cm) or vertical geometries that reduce field crowding at the dielectric-semiconductor interface. It is thus concluded the passivation material in our experiments caused premature breakdown. Regardless, this simple structure's ability to hold fields up to 2 MV/cm confirms the field



(a)



(b)



(c)

Fig. 4. (a) Block diagram of lifetime measurement set up using a pulsed 355 nm laser source illuminated on PCSS CPWs. (b) Measured waveforms of the PCSS CPW from 30 to 100 V bias, compared to the input laser waveform. (c) Lifetime calculated from the decay signals for varied input laser energy.

handling capability is high in Fe- β Ga₂O₃, which addresses an important need for PCSS devices.

B. Carrier Lifetime

Carrier lifetime was then measured using a modified probe station to support a 30 ps full-width half-maximum (FWHM) pulsed optical laser input (Ekspla PL2230, 355 nm) onto the CPW structures, similar to that of our previous work [27]. The block diagram of this measurement is depicted in Fig. 4(a) — several elements are included to ensure the oscilloscope is protected from a breakdown event. A static dc bias was applied across the signal trace in line with a 50 Ω load oscilloscope input (Keysight MSOV334A, 33 GHz, 80 GS/s). Various laser pulse energies (0.48–2.54 μJ at 355 nm) were tested. The waveform collected has a decaying tail, as seen in Fig. 4(b), and show the increase in magnitude with bias from 30 to 100 V. Lifetime was extracted from the log-linear slope of the decay. The calculated lifetimes over a range of electric fields and input laser energies are presented in Fig. 4(c). With a small variation in average electric field and laser energy, the carrier lifetime is estimated to be between 90 and 110 ps for a 355 nm optical input. This implies the trap mechanism for generating and combining the generated carriers in this sample is not heavily dependent on field or photon flux.

C. PCSS DC Behavior With Temperature

Dark current and responsivity measurements were then performed over temperature on a vertical PCSS structure [Fig. 2(c)]. A Keithley 4200 parameter analyzer was used to measure the photoresponsivity of the Fe- β Ga₂O₃ PCSS device. Both dark and photocurrent were measured by sweeping the voltage to 200 V and for temperature range of 25 $^{\circ}\text{C}$ –203 $^{\circ}\text{C}$. A 447 nm illumination wavelength light emitting diode (LED) was used to activate the sub-bandgap photo response of the

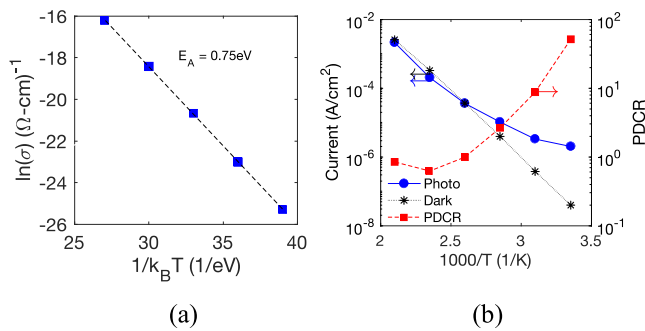


Fig. 5. Temperature characterization of the Fe- β Ga $_2$ O $_3$ PCSS. (a) Logarithmic plot with respect to temperature to extract activation energy of the sample. (b) Photograph and dark current and PDCR with respect to temperature at 200 V bias.

device. The incident power was monitored intermittently with an Ophir PD10-C power meter, with 150 mW being the target nominal value.

From the dark current, we calculated the sample conductivity as a function of temperature and extracted activation energy (E_A) using the Arrhenius equation

$$\sigma = \sigma_o \exp\left(-\frac{E_A}{k_B T}\right) \quad (1)$$

where σ is the electrical conductivity, σ_o is the preexponential factor, k_B is the Boltzmann's constant, and T is temperature. With our data, E_A is extracted to be 0.75 eV, which is in range of the reported Fe $^{2+/3+}$ trap level [11], [12], [13], [14], [15], [18], shown in Fig. 5(a). At high temperature, we saw a rapid increase in photocurrent up three orders of magnitude, in addition to a rapid decreased in photocurrent to dark current ratio (PDCR), reported in Fig. 5(b).

D. PCSS Pulsed Response With Varied Wavelengths

Three Teem Photonics pulsed lasers (355, 532, and 1064 nm) were fiber coupled and illuminated the vertical PCSS on a high voltage test board. The pulse widths and max energy for each laser were 0.6 ns with 1.61 μ J, 0.75 ns with 3.43 μ J, and 0.56 ns with 3.56 μ J, respectively. The illuminated spot size was estimated to be 1 mm diameter and neutral density filters were used to change the input intensity. The optical pulse triggers the vertical PCSS (biased at 100 V) to conduct and the corresponding current increase is measured across a 50 Ω oscilloscope channel. We calculated responsivity from the peak current scaled by the input energy pulse converted to peak power. Fig. 6(a) shows the responsivity at 100 V with respect to laser intensity, and the highest intensity output waveforms from each laser are shown in Fig. 6(b). The 1064 nm waveforms were quite small, close to the noise floor of the measurement equipment, so only the full laser energy was used in this measurement. As expected, the higher energy wavelengths had higher absorption efficiency and thus higher responsivity. These results will be discussed in the next section.

IV. DISCUSSION

A. PCSS Performance

The responsivity values scaled with electric field (R/E) are summarized in Table II. The highest value we measured for

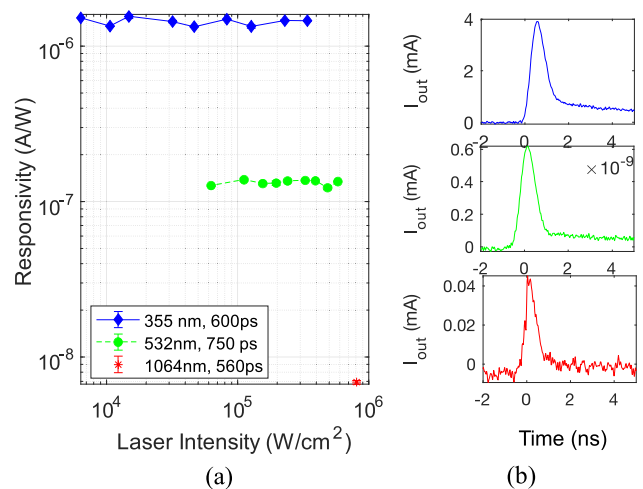


Fig. 6. (a) Responsivity at 100 V bias of the vertical PCSS device scaled with laser intensity for different wavelength sources. (b) Measured output waveform from each wavelength (top: 355 nm, middle: 532 nm, and bottom: 1064 nm) at the highest intensity tested for each.

TABLE II
SUMMARY OF Fe- β Ga $_2$ O $_3$ CHARACTERISTICS AS A PCSS

Input Wavelength (nm)	Absorption coefficient (cm $^{-1}$)	R/E (A-cm/W-kV)	Proposed Carrier Generation (Fig.7)
1064 (1.17eV)	1.02	3.1x10 $^{-9}$	(I) Only
532 (2.33 eV)	2.56	6.2x10 $^{-8}$	(I) Most, (II) Some
447 (2.77 eV)	3.41	5.2x10 $^{-7}$ (20°C) 5.49x10 $^{-4}$ (200°C)	(I) Few (II) Most
355 (3.49 eV)	5.97	6.9x10 $^{-7}$	(I) Few (II) Most

R/E at room temperature was 6.9×10^{-7} A-cm/W-kV at 355 nm. When we compare this with some recent PCSS devices in the literature, we see diamond PCSS has still the highest reported sub-bandgap R/E (2.5×10^{-4} A-cm/W-kV [28]) and SiC PCSS ($1.25e^{-5}$ A-cm/W-kV [29]) and GaN (1.75×10^{-5} A-cm/W-kV [30]) are relatively larger than the PCSS tested here, likely due to more efficient absorption of light in those experiments. Future work can focus on improving the external optical absorption efficiency of the Fe- β Ga $_2$ O $_3$ using reflectors and total internal reflection structures [3], [31].

While the absorption coefficient does not change much from the highest to lowest optical wavelengths (5.97–1.02), we see a more drastic change in R/E values. In addition, the increase in temperature shows an even further R/E increase to 5×10^{-4} A-cm/W-kV. This implies different traps are being activated at different wavelengths and temperatures, which will be elaborated upon in the next section.

B. Trap Model in Fe- β Ga $_2$ O $_3$

From these results, we see a few interesting observations. First, the absorption coefficient and the responsivity dependence on wavelength are not identical—implying there is a different interaction ratio of the possible transition states at different photon absorption levels. Theory shows the sub-bandgap absorption coefficient is related to the sum of the optical absorption cross section scaled with the population of each

deep level trap [32]. From this data, it is not possible to extract the absolute optical absorption cross section because it is unclear how many deep level traps are in use between the Fe and Ir (or other deep level defects not characterized in this study). The coefficient of absorption was only $6\times$ larger at 355 nm compared to 1064 nm, but the responsivity was 10^2 larger. This indicates that the deep level trap populations activated vary at different photon energies, with larger energies likely leading to both hole and electron excitation processes that can exhibit drastically different optical capture cross sections. [33], [34], [35].

In addition, we see a large increase in R/E with temperature by three orders of magnitude from 20 °C to 200 °C. The R/E increase was accompanied by a large increase in dark current due to the relatively low activation energy of Fe (0.75–0.8 eV)—the additional photocurrent implies other dopants and impurities are getting additionally ionized at these higher temperatures, and optically activated by the Fe²⁺ and Ir³⁺ traps. This could also include shallow donors that have been observed but not ionized at room temperature, such as the unknown 110 MeV donor [36]. This is consistent with the relatively larger population of unfilled Fe³⁺ traps available in this sample, being $10\times$ higher in concentration than the unintentionally doped Si.

The key optical absorption pathways are summarized in the band diagram in Fig. 7. It is assumed the shallow Si donor is fully compensated by the Fe dopant, so there are both Fe²⁺ and Fe³⁺ species in the sample at equilibrium. The lowest energy absorption path is the release of an electron to the CB, converting Fe²⁺ to Fe³⁺ (path I. in Fig. 7). While the Fe²⁺ level sits ~ 0.7 – 0.8 eV below the CB, it has been experimentally observed that absorption levels extend to 1.2–1.5 eV below CB for this trap due to relaxation energy in the lattice, with similar energetics predicted for Fe occupying both the tetrahedral and octahedral Ga sites [11]. Thus, the 1.17 eV optical energy of the 1064 nm light will cause very small fractions of transmission to the CB, which is consistent with the responsivity data in Table II. The higher energy optical sources tested were 2.3 eV and higher, which can activate absorption in the deep Ir³⁺ state and other deep donors and acceptors that may be present [34], [35]. Since Ir is a deep donor, its absorption of photons 2.3 eV and higher can lead to two different pathways—first direct emission of electrons to CB (path II. in Fig. 7) or a charge-transfer transition to Fe³⁺ or possibly another defect (path III. in Fig. 7). Zimmerman et al. [33] in 2020 showed relative optical absorption peaks for Fe in β Ga₂O₃ around 2.2 eV and decreases at higher energies, which implies the Fe²⁺ emission is more dominant in the 2.3 and 2.7 eV energies (green and blue) compared to the higher energy light. However, the higher responsivity with higher energies would suggest the Ir³⁺ optical cross section is likely larger at 3.49 eV compared to the Fe²⁺ optical cross section, or more deep level traps are likely being activated (perhaps Ga-vacancy related complexes, Cr-related complexes, or other intrinsic defects [15], [20], [34], [35], [36], [37]). Given the limited data available about Ir optical cross sections in β Ga₂O₃, this hypothesis could be investigated in future work.

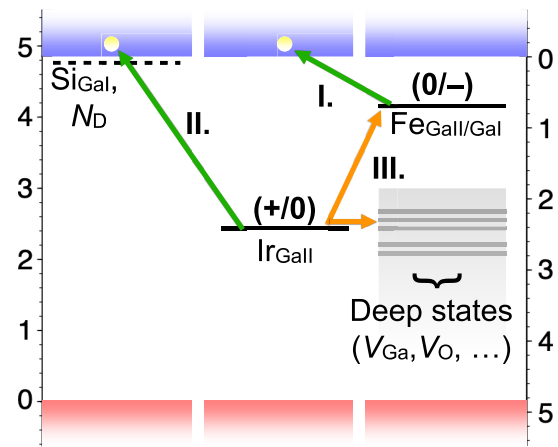


Fig. 7. Proposed trap model with active impurities in our sample. Green arrows correspond to carrier generation and yellow arrows correspond to internal transitions.

Further work should be done to study additional potential traps in more detail with both experimental characterization as well as theoretical modeling and dopant optimization of the PCSS performance. In addition, there should be further characterization of the carrier lifetime at different optical wavelengths and provide more insight into the trap model, as well as a higher electric field breakdown setup. In order to enable a PCSS for extreme environments, the high dark current in the sample needs to be addressed. It is thus recommended that different deep-level concentrations and deeper dopants, such as magnesium [11], [12], be explored in future work. Further device design and optimization would then be possible to realize a harsh environment β Ga₂O₃ PCSS.

V. CONCLUSION

We showed that Fe- β Ga₂O₃ has potential as a PCSS for high power switching. We first confirmed a large breakdown field >2 MV/cm, limited by the passivation materials in the lateral electrode experiment. We then characterized the free-carrier recombination lifetime of the sample with 355 nm input to be around 100 ps, which provides a means for high-speed switching. We also did a dc electrical characterization of the PCSS from room temperature to 200 °C and pulsed behavior at different wavelengths. While some advantages of β Ga₂O₃ include its lower cost compared to diamond and high responsivity at high temperature, the low photo to dark current ratio at 200 °C remains a disadvantage of this particular dopant-concentration profile. Regardless, this is the first demonstration of a β Ga₂O₃ PCSS which opens the path toward more optimal trap engineering to realize an extreme environment optical switch.

ACKNOWLEDGMENT

Wafers were purchased from Kyma Technologies, and microfabrication processing was done at the Center for Micro and Nano Technology at Lawrence Livermore National Laboratory. SIMS data were collected at Evans Analytical Group (EAG). The authors would like to thank Michael Crumb, Michael Rushford, and Victor Khitrov for their support with laser measurements.

REFERENCES

- [1] E. Majda-Zdancewicz, M. Suproniuk, M. Pawłowski, and M. Wierzbowski, "Current state of photoconductive semiconductor switch engineering," *Opto-Electron. Rev.*, vol. 26, no. 2, pp. 92–102, May 2018, doi: [10.1016/j.opelre.2018.02.003](https://doi.org/10.1016/j.opelre.2018.02.003).
- [2] S. K. Mazumder et al., "Overview of wide/ultra-wide bandgap power semiconductor devices for distributed energy resources," *IEEE J. Emerg. Sel. Topics Power Electron.*, vol. 11, no. 4, pp. 3957–3982, Aug. 2023, doi: [10.1109/JESTPE.2023.3277828](https://doi.org/10.1109/JESTPE.2023.3277828).
- [3] M. Bora et al., "A total internal reflection photoconductive switch," *IEEE Electron Device Lett.*, vol. 40, no. 5, pp. 734–737, May 2019, doi: [10.1109/LED.2019.2903926](https://doi.org/10.1109/LED.2019.2903926).
- [4] D. L. Hall et al., "Photoconductive switch with high sub-bandgap responsivity in nitrogen-doped diamond," *IEEE Electron Device Lett.*, vol. 41, no. 7, pp. 1070–1073, Jul. 2020, doi: [10.1109/LED.2020.2999821](https://doi.org/10.1109/LED.2020.2999821).
- [5] K. Woo, M. Malakoutian, B. A. Reeves, and S. Chowdhury, "A study on sub-bandgap photoexcitation in nitrogen- and boron-doped diamond with interdigitated device structure," *Appl. Phys. Lett.*, vol. 120, no. 11, Mar. 2022, Art. no. 112104, doi: [10.1063/5.0083710](https://doi.org/10.1063/5.0083710).
- [6] K. N. Heinselman, D. Haven, A. Zakutayev, and S. B. Reese, "Projected cost of gallium oxide wafers from edge-defined film-fed crystal growth," *Crystal Growth Des.*, vol. 22, no. 8, pp. 4854–4863, Jul. 2022, doi: [10.1021/acs.cgd.2c00340](https://doi.org/10.1021/acs.cgd.2c00340).
- [7] M. Higashiwaki, A. Kuramata, H. Murakami, and Y. Kumagai, "State-of-the-art technologies of gallium oxide power devices," *J. Phys. D, Appl. Phys.*, vol. 50, no. 33, Jul. 2017, Art. no. 333002, doi: [10.1088/1361-6463/aa7aff](https://doi.org/10.1088/1361-6463/aa7aff).
- [8] S. Poncé and F. Giustino, "Structural, electronic, elastic, power, and transport properties of β -Ga₂O₃ from first principles," *Phys. Rev. Res.*, vol. 2, no. 3, Jul. 2020, Art. no. 033102, doi: [10.1103/physrevresearch.2.033102](https://doi.org/10.1103/physrevresearch.2.033102).
- [9] M. E. Ingebrigtsen et al., "Iron and intrinsic deep level states in Ga₂O₃," *Appl. Phys. Lett.*, vol. 112, no. 4, Jan. 2018, Art. no. 042104, doi: [10.1063/1.5020134](https://doi.org/10.1063/1.5020134).
- [10] A. T. Neal et al., "Donors and deep acceptors in β -Ga₂O₃," *Appl. Phys. Lett.*, vol. 113, no. 6, Aug. 2018, Art. no. 062101, doi: [10.1063/1.5034474](https://doi.org/10.1063/1.5034474).
- [11] S. Bhandari, M. E. Zvanut, and J. B. Varley, "Optical absorption of Fe in doped Ga₂O₃," *J. Appl. Phys.*, vol. 126, no. 16, Oct. 2019, Art. no. 165703, doi: [10.1063/1.5124825](https://doi.org/10.1063/1.5124825).
- [12] S. Bhandari and M. E. Zvanut, "Charge trapping at Fe due to midgap levels in Ga₂O₃," *J. Appl. Phys.*, vol. 129, no. 8, Feb. 2021, Art. no. 085703, doi: [10.1063/5.0042622](https://doi.org/10.1063/5.0042622).
- [13] A. Y. Polyakov, V. I. Nikolaev, E. B. Yakimov, F. Ren, S. J. Pearton, and J. Kim, "Deep level defect states in β -, α -, and ϵ -Ga₂O₃ crystals and films: Impact on device performance," *J. Vac. Sci. Technol. A, Vac. Surf. Films*, vol. 40, no. 2, Mar. 2022, Art. no. 020804, doi: [10.1116/6.0001701](https://doi.org/10.1116/6.0001701).
- [14] J. F. MeGlone et al., "Trapping effects in Si δ -Doped β -Ga₂O₃ MESFETs on an Fe-doped β -Ga₂O₃ substrate," *IEEE Electron Device Lett.*, vol. 39, no. 7, pp. 1042–1045, Jul. 2018, doi: [10.1109/LED.2018.2843344](https://doi.org/10.1109/LED.2018.2843344).
- [15] Z. Wang, X. Chen, F.-F. Ren, S. Gu, and J. Ye, "Deep-level defects in gallium oxide," *J. Phys. D, Appl. Phys.*, vol. 54, no. 4, Nov. 2020, Art. no. 043002, doi: [10.1088/1361-6463/abb6b1](https://doi.org/10.1088/1361-6463/abb6b1).
- [16] J. R. Ritter, K. G. Lynn, and M. D. McCluskey, "Iridium-related complexes in Czochralski-grown β -Ga₂O₃," *J. Appl. Phys.*, vol. 126, no. 22, Dec. 2019, Art. no. 225705, doi: [10.1063/1.5129781](https://doi.org/10.1063/1.5129781).
- [17] Z. Galazka et al., "Czochralski growth and characterization of β -Ga₂O₃ single crystals," *Crystal Res. Technol.*, vol. 45, no. 12, pp. 1229–1236, Aug. 2010, doi: [10.1002/crat.201000341](https://doi.org/10.1002/crat.201000341).
- [18] M. D. McCluskey, "Point defects in Ga₂O₃," *J. Appl. Phys.*, vol. 127, no. 10, pp. 1–14, Mar. 2020, doi: [10.1063/1.5142195](https://doi.org/10.1063/1.5142195).
- [19] D. C. Look and J. H. Leach, "On the accurate determination of absorption coefficient from reflectance and transmittance measurements: Application to Fe-doped GaN," *J. Vac. Sci. Technol. B, Nanotechnol. Microelectron., Mater., Process., Meas., Phenomena*, vol. 34, no. 4, Jul. 2016, Art. no. 04J105, doi: [10.1116/1.4954211](https://doi.org/10.1116/1.4954211).
- [20] R. Sun, Y. K. Ooi, P. T. Dickens, K. G. Lynn, and M. A. Scarpulla, "On the origin of red luminescence from iron-doped β -Ga₂O₃ bulk crystals," *Appl. Phys. Lett.*, vol. 117, no. 5, Aug. 2020, Art. no. 052101, doi: [10.1063/5.0012967](https://doi.org/10.1063/5.0012967).
- [21] W. S. Yoo, K. Kang, G. Murai, and M. Yoshimoto, "Temperature dependence of photoluminescence spectra from crystalline silicon," *ECS J. Solid State Sci. Technol.*, vol. 4, no. 12, p. P456, 2015, doi: [10.1149/2.0251512jss](https://doi.org/10.1149/2.0251512jss).
- [22] N. Trinh, "Electrode design for testing in uniform field gaps," *IEEE Trans. Power App. Syst.*, vol. PAS-99, no. 3, pp. 1235–1242, May 1980, doi: [10.1109/TPAS.1980.319754](https://doi.org/10.1109/TPAS.1980.319754).
- [23] S. Diahm, S. Zemat, M.-L. Locatelli, S. Dinculescu, M. Decup, and T. Lebey, "Dielectric breakdown of polyimide films: Area, thickness and temperature dependence," *IEEE Trans. Dielectr. Electr. Insul.*, vol. 17, no. 1, pp. 18–27, Feb. 2010, doi: [10.1109/TDEI.2010.5411997](https://doi.org/10.1109/TDEI.2010.5411997).
- [24] 3M. (Sep. 2019). *3M Fluorinert Electronic Liquid FC-40*. 3M Electronics Materials Solutions Division, St. Paul, MN USA. Accessed: Oct. 20, 2023. [Online]. Available: <https://multimedia.3m.com/mws/media/648880/3m-fluorinert-electronic-liquid-fc40.pdf>
- [25] X. Yan, I. S. Esqueda, J. Ma, J. Tice, and H. Wang, "High breakdown electric field in β -Ga₂O₃/graphene vertical barristor heterostructure," *Appl. Phys. Lett.*, vol. 112, no. 3, Jan. 2018, Art. no. 032101, doi: [10.1063/1.5002138](https://doi.org/10.1063/1.5002138).
- [26] A. J. Green et al., " β -gallium oxide power electronics," *APL Mater.*, vol. 10, no. 2, Feb. 2022, Art. no. 029201, doi: [10.1063/5.0060327](https://doi.org/10.1063/5.0060327).
- [27] K. Dowling et al., "Pulse compression photoconductive switching using negative differential mobility," *IEEE Trans. Electron Devices*, vol. 69, no. 2, pp. 590–596, Feb. 2022, doi: [10.1109/TED.2021.3136500](https://doi.org/10.1109/TED.2021.3136500).
- [28] P. K. Bharadwaj, R. F. Code, H. M. van Driel, and E. Walentynowicz, "High voltage optoelectronic switching in diamond," *Appl. Phys. Lett.*, vol. 43, no. 2, pp. 207–209, Jul. 1983, doi: [10.1063/1.94288](https://doi.org/10.1063/1.94288).
- [29] J. S. Sullivan and J. R. Stanley, "6H-SiC photoconductive switches triggered at below bandgap wavelengths," *IEEE Trans. Dielectr. Electr. Insul.*, vol. 14, no. 4, pp. 980–985, Aug. 2007, doi: [10.1109/TDEI.2007](https://doi.org/10.1109/TDEI.2007).
- [30] J. S. Sullivan and J. R. Stanley, "Wide bandgap extrinsic photoconductive switches," *IEEE Trans. Plasma Sci.*, vol. 36, no. 5, pp. 2528–2532, Oct. 2008, doi: [10.1109/TPS.2008.2002147](https://doi.org/10.1109/TPS.2008.2002147).
- [31] X. Yang et al., "Improved photocurrent for gallium nitride photoconductive semiconductor switch by SiO₂ anti-reflection and (SiO₂|Ta₂O₅)⁶ high-reflection dielectric films," *IEEE Electron Device Lett.*, vol. 44, no. 10, pp. 1696–1699, Oct. 2023, doi: [10.1109/LED.2023.3301912](https://doi.org/10.1109/LED.2023.3301912).
- [32] A. Alkauskas, M. D. McCluskey, and C. G. Van de Walle, "Tutorial: Defects in semiconductors—Combining experiment and theory," *J. Appl. Phys.*, vol. 119, no. 18, May 2016, Art. no. 181101, doi: [10.1063/1.4948245](https://doi.org/10.1063/1.4948245).
- [33] C. Zimmermann, Y. Kalmann Frodason, V. Rønning, J. B. Varley, and L. Vines, "Combining steady-state photo-capacitance spectra with first-principles calculations: The case of Fe and Ti in β -Ga₂O₃," *New J. Phys.*, vol. 22, no. 6, Jun. 2020, Art. no. 063033, doi: [10.1088/1367-2630/ab8e5b](https://doi.org/10.1088/1367-2630/ab8e5b).
- [34] A. Singh et al., "Ultrafast dynamics of gallium vacancy charge states in β -Ga₂O₃," *Phys. Rev. Res.*, vol. 3, no. 2, May 2021, Art. no. 023154, doi: [10.1103/physrevresearch.3.023154](https://doi.org/10.1103/physrevresearch.3.023154).
- [35] Y. Fang et al., "Native defect-related broadband ultrafast photocarrier dynamics in n-type β -Ga₂O₃," *Appl. Phys. Lett.*, vol. 121, no. 11, Sep. 2022, Art. no. 113103, doi: [10.1063/5.10100190](https://doi.org/10.1063/5.10100190).
- [36] A. T. Neal et al., "Incomplete ionization of a 110 meV unintentional donor in β -Ga₂O₃ and its effect on power devices," *Sci. Rep.*, vol. 7, no. 1, p. 13218, Oct. 2017, doi: [10.1038/s41598-017-13656-x](https://doi.org/10.1038/s41598-017-13656-x).
- [37] Y. K. Frodason, C. Zimmermann, E. F. Verhoeven, P. M. Weiser, L. Vines, and J. B. Varley, "Multistability of isolated and hydrogenated Ga–O divacancies in β -Ga₂O₃," *Phys. Rev. Mater.*, vol. 5, no. 2, Feb. 2021, Art. no. 025402, doi: [10.1103/physrevmaterials.5.025402](https://doi.org/10.1103/physrevmaterials.5.025402).